Simple Modeling and Prototype Experiments for a New High-Thrust Low-Speed Permanent-Magnet Disk Motor

Genevieve Patterson, Takafumi Koseki, *Member, IEEE*, Yasuaki Aoyama, and Kentaro Sako

***Abstract*—Fully integrated electric propulsion systems are gaining popularity in both commercial and military sectors. Propulsion motor manufacturers are investigating new direct-drive solutions for use in electric ships. These applications require motors with high torque output at low speeds. Such requirements were the motivation for the design of a new permanent-magnet synchronous motor (PMSM) with a novel topology. This paper describes the efficient mathematical model used to optimize our PMSM design. Based on a simplified theoretical model for the motor's behavior, we were able to quickly and accurately predict torque output. The minimalist design of this transverse flux machine is shown to be advantageous for computer simulation and machine manufacturing. Initial results from a prototype are included and discussed. Future plans for the prototype are outlined.**

***Index Terms*—Electric propulsion, permanent-magnet synchronous motor (PMSM), transverse flux machine (TFM), tunnel actuator (TA).**

I. Introduction

JUST as the commercial automotive, aerospace, and railway industries have been affected by rising fuel costs, the marine industry has recently endeavored to create more fuel-efficient cost-effective drive systems. During the last 15–20 years, fully electrified propulsion (EP) systems have been gaining popularity and capturing most of the market growth in sectors such as cruise ships, passenger ferries, oil and gas transport vessels, and merchant and special order ships [1], [2]. The popularity of EP is due to savings in onboard space, fuel, electrical losses, noise and vibrations, and maintenance.

Manuscript received February 18, 2010; accepted May 14, 2010. Date of publication November 15, 2010; date of current version January 19, 2011. Paper 2010-EMC-045, presented at the 2009 International Conference on Electrical Machines and Systems, Tokyo, Japan, November 15–18, and approved for publication in the IEEE Transactions on Industry Applications by the Electric Machines Committee of the IEEE Industry Applications Society. This paper was supported in part by the Japan Society for the Promotion of Science through the 2009 Grant-in-Aid for Scientific Research program.

G. Patterson was with the Department of Electrical Engineering and Information Systems, The University of Tokyo, Tokyo 113-8656, Japan. She is now with Brown University, Providence, RI 02912 USA (e-mail: Patterson.genevieve@gmail.com).

T. Koseki is with the Department of Electrical Engineering and Information Systems, The University of Tokyo, Tokyo 113-8656, Japan (e-mail: takafumikoseki@gmail.com).

Y. Aoyama is with the Hitachi Research Laboratory, Hitachi, Ltd., Ibaraki Prefecture 319-1292, Japan (e-mail: Yasuaki.aoyama.fq@hitachi.com).

K. Sako was with the Department of Electrical Engineering and Information Systems, The University of Tokyo, Tokyo 113-8656, Japan and is now with Honda Motors, Mie Prefecture 510-1312, Japan (e-mail: ktrs82@gmail.com).

Color versions of one or more of the figures in this paper are available online at http://ieeexplore.ieee.org.

Digital Object Identifier 10.1109/TIA.2010.2090933

Several different types of motors are currently in use or have been proposed for application in ship propulsion. We took particular interest in a permanent-magnet synchronous motor (PMSM) solution because of the possibility of higher thrust, less complicated design, and lower maintenance when compared with induction motor solutions. PMSMs are also much less expensive than high-temperature superconductor machines.

Due to the short pole-pitch characteristic of certain types of PMSM designs, these machines can have high torque at low speeds, which is particularly beneficial in a marine application. Transverse flux motor designs have short pole-pitch and high torque characteristics, but TFMs are plagued by low power factor [3]. In order to improve on previous designs, we developed a theoretical model of a transverse flux PMSM and subsequently built and tested the prototype of a new design. We also adapted the basic flux path idea present in the Tunnel Actuator, a linear PMSM produced by Hitachi, to perform in a rotary application.

II. Fundamentals of the New Motor Design

The transverse flux machine takes advantage of a 3-D flux path to increase torque production without having to tradeoff between electrical or magnetic loading as with radial and axial flux machines. However, the TFM described by Weh *et al.* and later improvements on that design have such complex manufacturing requirements that they are impractical for industrial production [4]. This complex design can be seen in Fig. 1. Ultimately, the low power-factor characteristic of transverse flux machines becomes an obstacle against this type of machine attaining high real power to volume ratio [3]. For example, Rolls-Royce Ltd. manufactured a TFM for marine propulsion that was capable of large thrust but had power-factor ratings of less than 0.7 [6].

When examining the field of direct drives for another motor with a similar flux path configuration but a high power factor, we found Hitachi's Tunnel Actuator, now available commercially as the H type Motor, for linear-drive applications [5]. This drive has the advantages of easy assembly, thin permanent magnet and high resultant permeability, and a magnetic flux path that is transverse. The Tunnel Actuator suffered from large leakage flux due to the close position of the armature poles and the configuration of the flux path in alternating poles. We thought that by placing only poles with flux in the same direction next to each other and spacing them further apart to increase magnetic isolation, we could create a better design. The following sections will show the details of our new direct-drive design.

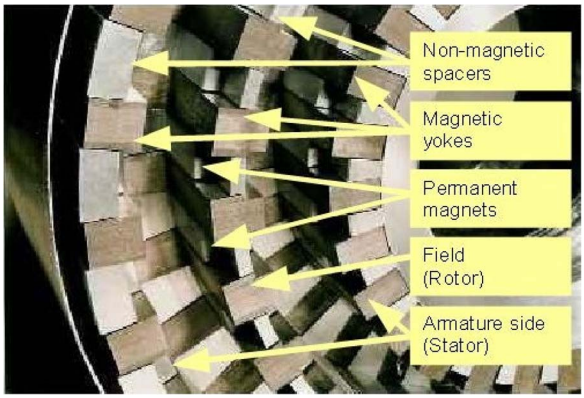

Fig. 1. Transverse flux machine.

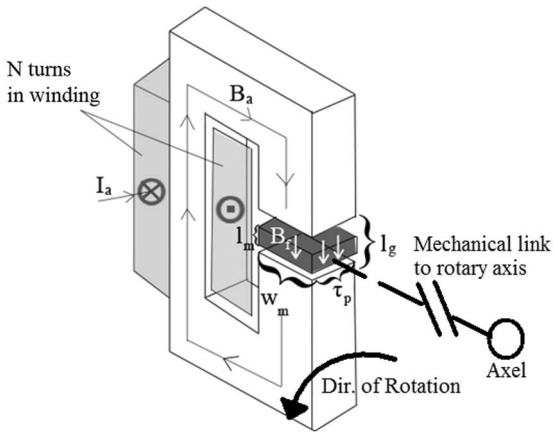

Fig. 2. One-pole model diagram.

A. One-Pole Model

The theoretical model for our machine was created by breaking down a transverse flux PMSM into its fundamental components. The basic unit of the model was one pole of the machine. A whole motor would have n poles per phase and m number of phases.

One pole consists of a stator C-core, where an air gap makes the break in the "C." The winding is wrapped around the back of the C, and the permanent magnets on the rotor are accelerated through the air gap to generate thrust. An illustration of the one-pole model is in Fig. 2. The input to the model is the armature current I_a. B_a is the armature flux, and B_f is the flux contributed by the field magnets. As I_a changes, the polarity of B_a also fluctuates, which pulls the alternating polarity magnets through the air gap, creating thrust. The movement of the magnets through the armature flux field also induces an internal electromotive force (EMF).

Fig. 3 shows how the rotor would be propelled through the consecutive air gaps of several poles connected in phase by their armature winding. The self-induced voltage and thrust contributed by each pole would be superimposed to create the total contribution of one phase. The phases of the machine could then be connected to the operator's convenience. The C-cores of each phase would be placed at balanced angular separation around the axel to create the outer radius of the machine. An illustration of a full version of the machine is shown in Fig. 7.

B. Per Phase Quasi-Stationary Equivalent Circuit Models

Fig. 4 shows the per phase equivalent circuit for a three-phase machine composed of n-connected C-cores. L_s and R_s are the synchronous armature inductance and resistance, respectively, but for the sake of simplicity, R_s is ignored in the following calculations. V_0 is the induced EMF, and $V_a$is the armature voltage.

Assuming that the motor has an n number of poles per phase and a three-phase star connection, (1)–(6) show how the armature voltage V_a, the synchronous impedance voltage drop V_s, and the self-induced voltage V_0 are calculated. The per phase armature self-inductance L_a and three-phase synchronous inductance L_s are inversely proportional to the air-gap length l_g, as shown in (2)–(4). L_s is twice as L_a because there are two stator poles per phase. This model neglects lossy elements because low losses are expected due to the magnetic isolation of the separate C-cores.

In (4)–(6), S is the surface area of the permanent magnet (PM), and ω_e is the synchronous angular speed. β is a form factor for matching the realistically jagged V_0 signal to a fundamental frequency. Equation (10) determines the PM flux density, which depends inversely on the magnet reluctance. Equation (11) determines the armature flux density, and B_a has the same inverse proportionality to air-gap reluctance

$$V = R_s * I_a + L_s \frac{dI_a(t)}{dt} + V_0 \tag{1}$$
$$V_s = L_s \omega_e I_a \tag{2}$$
$$L_s = 2 * L_a \tag{3}$$
$$L_a = N^2/R \tag{4}$$
$$R = \frac{l_g}{\mu_0 S} \tag{5}$$
$$V_0 = 3/2\beta\ SNB_f\omega_e \tag{6}$$
$$\Phi_f = \frac{H_c * l_m}{R\text{magnet}} \tag{7}$$
$$\Phi_a = \frac{Nia}{R\text{gap}} \tag{8}$$
$$\Phi_{\text{total}} = \Phi_a + \Phi_f \tag{9}$$
$$B_f = \frac{\Phi_f}{S} \tag{10}$$
$$B_a = \frac{\Phi_a}{S} \tag{11}$$
$$F = 3/2\beta\ B_a H_c l_m w_m. \tag{12}$$

This mathematical model is predicated on the idea of superposition. The magnetic flux, flux linkage, and induced voltage are all calculated for the unit core. The value for the whole machine is later calculated as multiple of the cores per phase and the number of phases in the motor. The total magnetic flux present in a single unit loop is also calculated as the superposition of the flux due to the armature winding plus the flux due to the permanent magnet.

Fig. 5 illustrates how the magnetic circuit model uses superposition. We chose to model the magnetic circuits as seen from the armature and field perspectives separately. The total magnetic flux is then a summation of the flux due to the armature winding and that due to the field magnet. Refer to (7)–(9) for a mathematical description of this relationship.

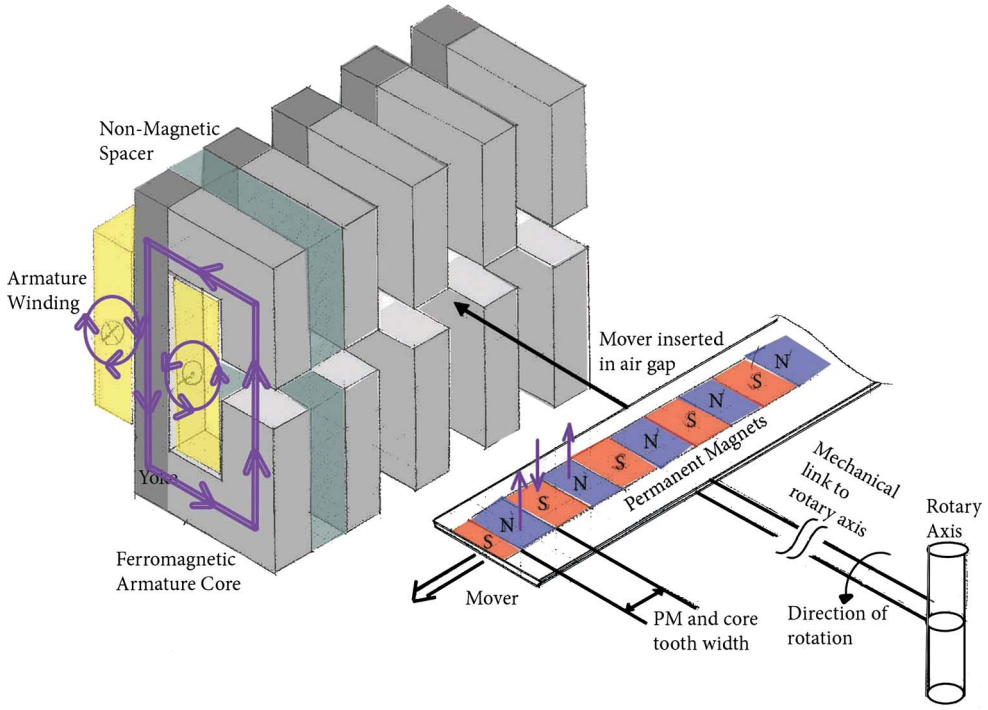

Fig. 3. Flux path through the C-core and rotor.

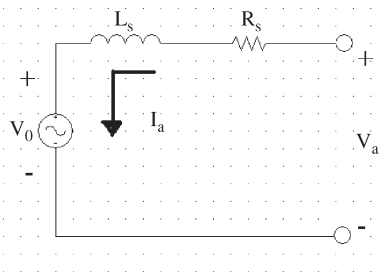

Fig. 4. Per phase equivalent circuit model.

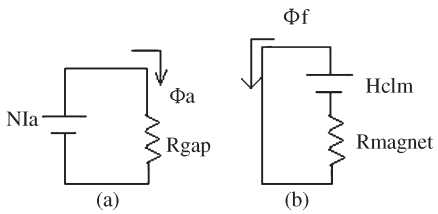

Fig. 5. Motor magnetic circuit model. (a) Armature magnetic circuit. (b) Field magnetic circuit.

However, a difficulty arises in this superposition. When the permanent magnet is not perfectly aligned with the ferromagnetic core, it does not contribute its full flux capability to the total flux value. This model treats the permanent magnet as a virtual coreless coil that can be divided easily without effecting the basic physical equations.

Equation (12) shows the thrust force produced by the whole three-phase machine. If the mechanical clearance, i.e, the space in the air gap not occupied by the magnet, is a value significantly smaller than l_m, then l_m and l_g are approximately the same. Thus, increasing l_m while keeping all other factors constant will not significantly increase thrust. The whole volume

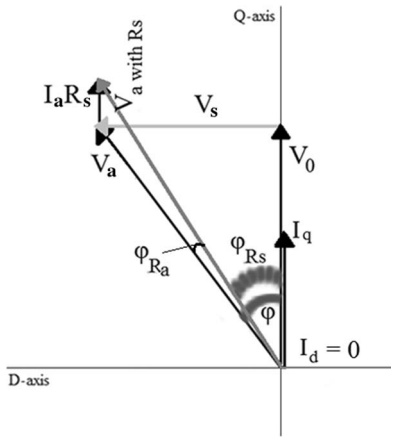

Fig. 6. Phasor diagram for a symmetrical three-phase machine.

of the magnet is effectively controlled by $l_m w_m$ because the pole pitch must remain in a constant value for a given input frequency. Magnet volume or its excitation strength, indicated by H_c, must increase in order to raise F. Equations (7) and (8) indicate that if a larger mechanical clearance is necessary, then the designer must accept lower flux density.

C. Power Factor and Thrust Calculation

In order to determine the power factor for the basic unit model, Fig. 6 shows the phasor diagram for the three-phase configuration's synthesized voltage vectors. In Fig. 6, the angles φ_{Ra} and φ are the power factor angles considering armature resistance and disregarding it, respectively. The value of φ_{Ra} would always be smaller than φ regardless of the value of the armature resistance, thus real-world PF values may be slightly better than those estimated by the model in this paper. Future research will likely include consideration of R_a.

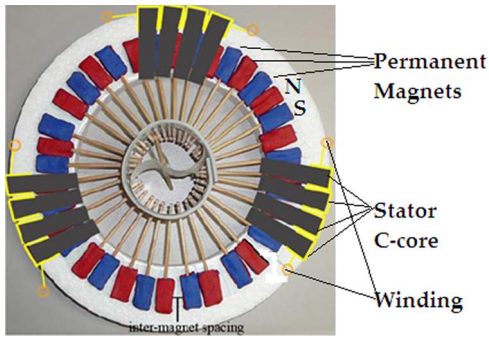

Fig. 7. Illustration of a rotary disk motor design concept.

Equations (13) and (14) show how the power factor and power-factor angle are calculated. It is important to note that φ is not dependent on the input frequency, as shown in (14). This indicates that ω_e can be increased, which increases the output thrust, but the power factor will remain the same. The absolute values of the internal voltages will, however, increase.

$$p.f. = \cos\varphi \tag{13}$$

$$\tan\varphi = \frac{V_s}{V_0} = \frac{3\mu_0 N I_a}{2\beta H_c l_m} = \frac{lgF}{\beta H_c^2 l_m^2 w_m} \tag{14}$$

$$I_a = \frac{2l_g F}{3N\mu_0 H_c l_m w_m}. \tag{15}$$

Assuming $l_g \cong l_m$, then

$$\tan\varphi = \frac{F}{\beta H_c^2 l_m w_m}. \tag{16}$$

Using the expression for I_a in (15), the formula in (16) illustrates the relationship between the power-factor angle and the thrust. If the volume and strength of the magnet are constant, when thrust F raises, the power factor lessens. The model verifies that there is an unavoidable tradeoff between power factor and thrust when the permanent-magnet excitation is constant.

III. Creation of the Prototype and Test Bench

The prototype design was created by taking a number of unit model C-cores and arranging them radially to create a full stator. In Fig. 7, this idea is drawn up with three phases and four stator cores per phase. In the actual prototype, only two cores were used per phase. The rotor was constructed in a similar fashion by placing alternating polarity magnets on a rotor backing at a set angular separation. In the prototype, there were 36 PMs, thus 18 pole pairs.

It is important to note that because the flux lines in adjacent stator cores of the same phase point in the same direction and there is a large physical separation between phases, we expected negligible leakage flux.

Fig. 8 is a photograph of the actual prototype. It was observed during the setup of this prototype that the precise positioning of the stator cores was significant. As previously mentioned, one of the fundamentals of the mathematical model was that the flux contribution from each C-core could be simply added by superposition. This assumption fails if the stator cores are not perfectly in phase. The in-phase position of the stator cores needs to be more precise the closer together the rotor magnets are, and because this was a small scale prototype, the acceptable positioning error was quite small.

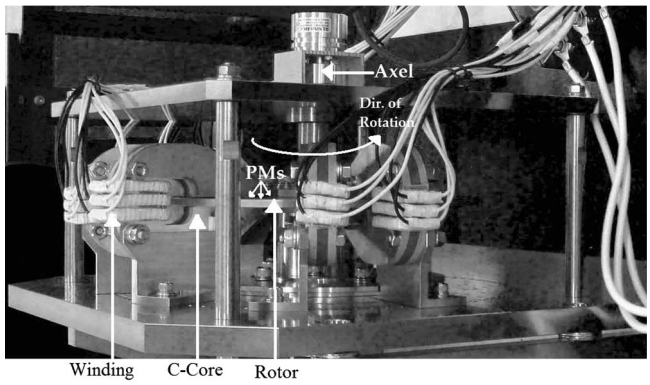

Fig. 8. Prototype motor.

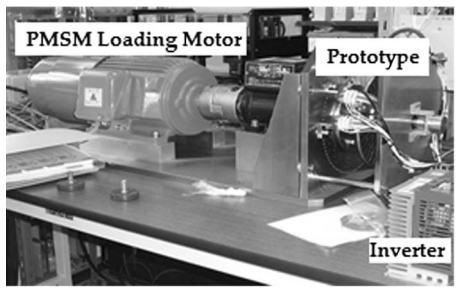

Fig. 9. Prototype test bench.

The full test bench, as shown in Fig. 9, involved directly connecting a PMSM load motor to the prototype. The prototype was driven directly in generator mode during the open circuit testing in Section IV. The prototype was connected to an inverter to be controlled for dynamic testing. This test bench accurately represents the typical case of an industrial client, where the motor supplier will have only general knowledge about the loading conditions applied to their product.

IV. No Load and Quasi-Stationary Testing

There were two phases to the machine characterization testing. These two tests will be outline in the subsequent sections.

A. Open Circuit Test

First, the open circuit voltage was measured. This test is crucial for identifying internal reversed EMF as a function of speed. This characteristic is used to calculate the motor constant used in the speed controller. The motor constant is the most significant performance index of the motor.

Fig. 10 shows the test circuit for this stage. The "Ch 1" reference shows how this circuit was connected to the scope. V_0 represents the back EMF.

During testing, the prototype's most stable operating range was at approximately 50-Hz input frequency. Fig. 11 demonstrates that the empirical values for V_0 at this speed are slightly less than the theoretical calculations. This is a reasonable expectation because the theoretical V_0 was calculated using the maximum flux density possible in the air gap. This peak value

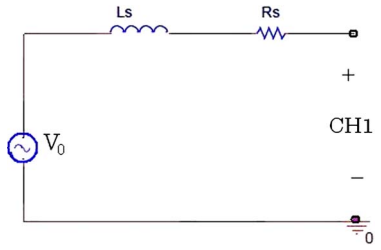

Fig. 10. Open circuit test circuit with oscilloscope connection label.

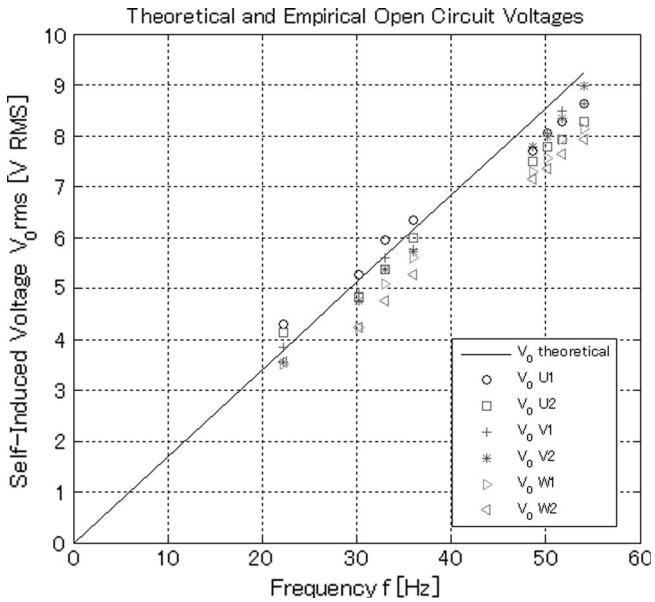

Fig. 11. Per pole open circuit voltage.

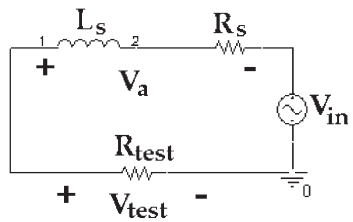

Fig. 12. Stationary ac input armature impedance test circuit.

is less in reality because the flux output is forced to approximate a sinusoidal waveform.

B. Stationary Rotor Direct and Quadrature Axis Armature Inductance Test

The stationary armature impedance test was completed in order to identify the real and imaginary internal synchronous impedances. A dc test to measure the armature resistance and an adaptation of the short circuit test commonly described in electromechanical machine literature would be optional to confirm the results of this test.

The test circuit is given in Fig. 12.

$$Z_s = \frac{V_a^{e^{i\theta}}}{V_{\text{test}}/R_{\text{test}}} \tag{17}$$

$$\theta = 2 * \pi * \frac{\tau}{T} \tag{18}$$

$$Z_s = R_s + j * \omega * L_s. \tag{19}$$

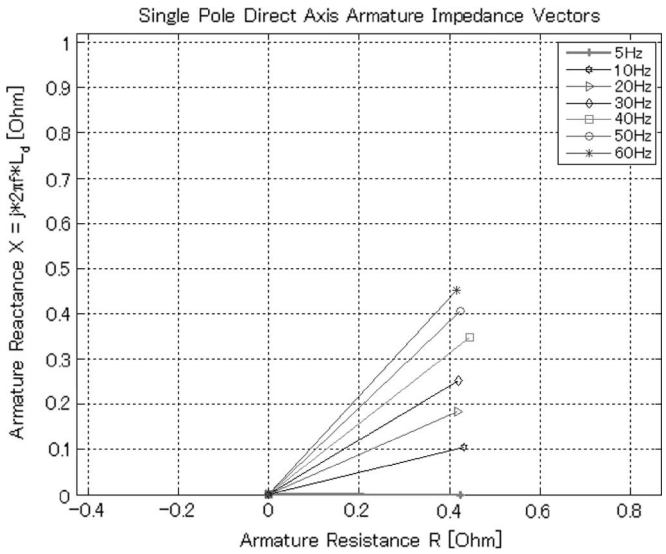

Fig. 13. Per pole direct axis complex impedance vectors for a range of input frequencies.

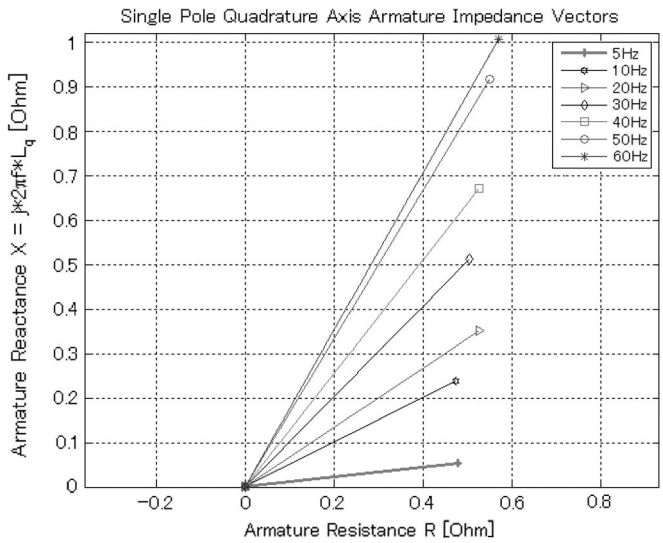

Fig. 14. Per pole quadrature axis complex impedance vectors for a range of input frequencies.

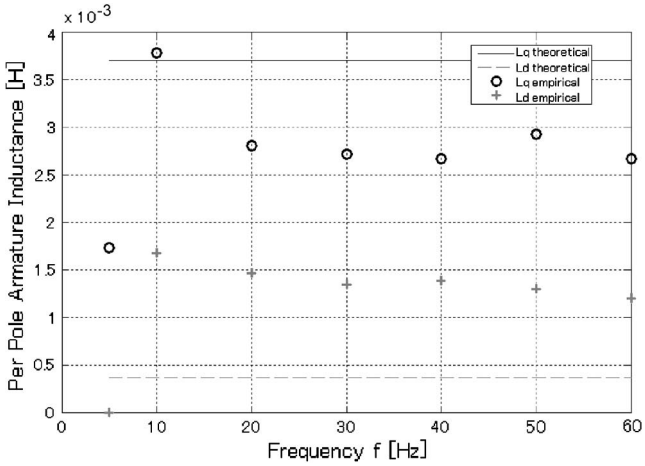

Fig. 15. Per pole direct axis complex impedance vectors for a range of input frequencies.

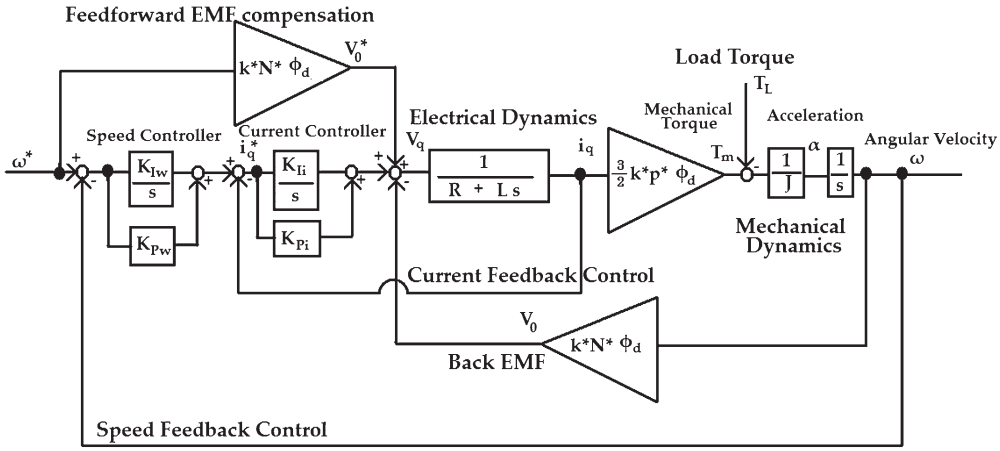

Fig. 16. Cascaded PI speed controller and Q-axis current controller.

The open layout of the prototype made it possible to observe if the rotor was stopped with the PM aligned with the stator core (d-axis) or 90° out of alignment (q-axis). Figs. 13 and 14 show the complex impedance vector at different frequencies. It is significant that the real axis values for each vector, i.e., the armature resistance value, are close to 0.43 Ω for each vector in both the d-axis and q-axis cases, although the q-axis values are slightly more.

Fig. 15 compares the theoretical and empirical values for armature inductance per pole. Equations (3) and (4) show how the theoretical values were calculated, except that for the q-axis value, ten times the permeability of free space was assumed for the rotor backing material. At the motor's stable operating frequency, the values for L_d and L_q are almost constant and within theoretical limits.

V. Speed Control and Dynamic Performance Expectations

A. Speed and Current Controller

The speed controller designed for the prototype was a conventional cascade controller using the parameters calculated in the last section for the motor's plant model. There were three steps in the construction of this controller. The first was the three-phase ac input to two-phase direct/quadrature input transformation. The second step was to make a PI controller with feedforward EMF compensation. The third part was a PI speed controller for suppressing the effects of load torque. C. Kessler's canonical form was used to calculate the PI gains. The motor constant was calculated from the open circuit test.

Fig. 16 shows the outline of the controller without the three-phase to two-phase transformation. This model assumes that the motor is nonsalient pole, and $I_d = 0$. Thus, only the Q-axis relationships are shown in Fig. 16.

B. Planned Dynamic Testing and Anticipated Results

Table I shows the theoretical and empirical values for the efficiency, power factor, torque, and force density of the prototype. Due to the agreement of the simulated values for V_0 and Z_s, the expectation is that the dynamic behavior will also match

TABLE I
Comparison of Theoretical and Empirical Data

Variable	Theoretical Value	Empirical Value
frequency	50 Hz	50 Hz
N	84	84
L_s=2* (L_d+L_q)/2	4.16 mH	3.86 mH
R_s	0.75 Ω	0.75 Ω
I_a	4 A	4 A
V_0	9.78 V RMS	14.85 V RMS
V_a	14.04 V RMS	18.88 V RMS
Φ_f	5.24×10^{-4} Wb	7.96×10^{-4} Wb
B_f	0.44 T	0.66 T
B_a	4.98×10^{-4} T	4.98×10^{-4} T*
PF	0.93	0.97*
η	0.70	0.79*
$P_{mechanical}$	117.38 W	178.19 W*
Torque	6.73 Nm	10.21 Nm*
Force Density	50 kN/m^2 = 0.49 atm	75.6 kN/m^2 = 0.75atm*

*values are estimated based on empirical values for V_0 and Z_s

predictions. The torque and force density are high for this type of machine, and thus, the results are encouraging. The tradeoff between torque and power factor are also made obvious. An operating point of 50 Hz was selected because that is the typical operating frequency of electric ships.

The data from Table I are encouraging because of the high thrust and power factor. It is expected that, by increasing the armature winding number, it would be possible to improve the efficiency in later prototypes.

VI. Conclusion

This paper has proposed a new evolution in the development of the transverse-flux-type permanent-magnet motor. A new idea for a low-speed high-torque permanent-magnet motor has been proposed. We reviewed the initial transverse flux concept and the two adaptations of the TFM topology. The concept outlined by Husband and Hodge in [6] gave encouraging results about the possibility of applying a direct-drive solution to electric ship propulsion but presented difficulties in the complexity of manufacturing and in a low power factor characteristic.

The new design introduced in this paper reimagines the transverse flux path. It has a simple flux topology that allowed for simplified linear modeling of the motor characteristics. The fundamental stationary characteristics of the new motor design were estimated analytically based on an elementary magnetic circuit analysis.

In the process of developing the mathematical model for this motor, the unavoidable tradeoff between thrust and power factor in a TFM was confronted. The linearity of our model allowed for a direct examination of this compromise that has been observed in the literature of TFM development.

In Section III, the original plan for a prototype has been presented. Although the layout of the machine and test bench lent itself well to rapid construction and direct measurement techniques, the placement of the stator cores had to be carefully planned to prevent torque ripple. The angular positioning of the C-cores has been the most significant step in preparing the prototype for stationary and running tests.

The fundamental measurements of the prototype's open circuit voltage and armature impedance have been completed successfully in Section IV. The results of these measurements have verified the accuracy of the mathematical model presented in Section II. The prognosis of these motor parameters has contributed to the speed controller design for the prototype motor.

At the time of publication, the plan for future work on this project has been clear. Dynamic testing must be conducted to verify the expectations presented in Section V. The next step we will take is to propose an improvement to the initial design in order to reduce the possibility of torque ripple and increase the ease of assembly. The results of dynamic testing and future prototype design may be presented at the time of the conference.

ACKNOWLEDGMENT

The authors would like to thank the members of the Hitachi Research Laboratory for their technical advice in support of this research.

REFERENCES

[1] J. Borman and B. Sharman, "Electric propulsion of passenger ships and other vessels," *Trans. ImarE*, vol. 106, pp. 77–104, Nov. 16, 1993.

[2] ABB, ABB Marine—References, Helsinki, Finland, Dec. 2006. [Online]. Available: www.abb.com/marine

[3] M. R. Harris, G. H. Pajooman, and S. M. Abu Sharkh, "The problem of power factor in VRPM (transverse-flux) machines," in *Proc. IEEE Conf. Elect. Mach. Drives, (Conf. Publ. No. 444)*, Sep. 1997, pp. 386–390.

[4] H. Weh, H. Hoffman, and J. Landrath, "New permanent magnet excited synchronous machine with high efficiency at low speeds," in *Proc. Int. Conf. Elect. Mach.*, 1988, pp. 35–40.

[5] H. J. Kim, J. Nakatsugawa, K. Sakai, and H. Shibata, "High-acceleration linear motor, 'Tunnel Actuator'," *J. Magn. Soc. Jpn.*, vol. 29, no. 3, pp. 199–204, 2005.

[6] S. M. Husband and C. G. Hodge, "The Rolls-Royce transverse flux motor development," in *Proc. IEEE Elect. Mach. Drives Conf.*, 2003, vol. 3, pp. 1435–1440.

Genevieve Patterson received the B.S. degree in electrical engineering and mathematics from the University of Arizona, Tucson, in 2007, and the Master of Electrical Engineering degree from The University of Tokyo, Tokyo, Japan, in 2009, in the laboratory of Prof. T. Koseki. She is currently working toward the Ph.D. degree in computer science at Brown University, Providence, RI.

Her interests include new mathematical techniques for applications in computer vision.

Takafumi Koseki (S'87–M'92) received the Ph.D. degree in electrical engineering from The University of Tokyo, Tokyo, Japan, in 1992.

He is currently an Associate Professor with the Department of Electrical Engineering and Information Systems, The University of Tokyo. His current research interests include public transport systems, particularly linear drives and the analysis and control of traction systems.

Dr. Koseki is a member of the Institute of Electrical Engineers of Japan, the Japan Society of Mechanical Engineering, the Japan Society of Applied Electromagnetics and Mechanics, and Verein Deutscher Ingenieure.

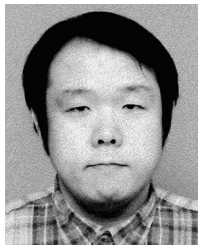

Yasuaki Aoyama received the M.S. degree from Tokyo University of Science, Tokyo, Japan, in 1998.

He has been with Hitachi Ltd., Tokyo, since 2007. He is currently with the Hitachi Research Laboratory, Tokyo, where he is involved in linear drives and rotating machine research and development.

Kentaro Sako received the B.S. degree in electrical engineering and information systems from The University of Tokyo, Tokyo, Japan, in 2010. His thesis research involves designing, building, and testing an improved second prototype of the transverse flux PMSM described in this paper.

He is currently an Engineer with Honda Motors, Tokyo.